

Can soaked-in scavengers protect metalloprotein active sites from reduction during data collection?

Sofia Macedo,^a Maria Pechlaner,^a Walther Schmid,^b Martin Weik,^c Katsuko Sato,^d Christopher Dennison^d and Kristina Djinović-Carugo^{a*}

^aDepartment for Structural and Computational Biology, Max F. Perutz Laboratories, University of Vienna, Campus Vienna Biocenter 5, 1030 Vienna, Austria, ^bInstitute of Organic Chemistry, University of Vienna, Währinger Strasse 38, 1090 Vienna, Austria, ^cLaboratoire de Biophysique Moléculaire, Institut de Biologie Structurale J.-P. Ebel, CEA CNRS UJF, UMR 5075, 41 rue Jules Horowitz, 38027 Grenoble Cedex 01, France, and ^dInstitute for Cell and Molecular Biosciences, Medical School, Newcastle University, Newcastle upon Tyne NE2 4HH, UK.
E-mail: kristina.djinovic@univie.ac.at

One of the first events taking place when a crystal of a metalloprotein is exposed to X-ray radiation is photoreduction of the metal centres. The oxidation state of a metal cannot always be determined from routine X-ray diffraction experiments alone, but it may have a crucial impact on the metal's environment and on the analysis of the structural data when considering the functional mechanism of a metalloenzyme. Here, UV–Vis microspectrophotometry is used to test the efficacy of selected scavengers in reducing the undesirable photoreduction of the iron and copper centres in myoglobin and azurin, respectively, and X-ray crystallography to assess their capacity of mitigating global and specific radiation damage effects. UV–Vis absorption spectra of native crystals, as well as those soaked in 18 different radioprotectants, show dramatic metal reduction occurring in the first 60 s of irradiation with an X-ray beam from a third-generation synchrotron source. Among the tested radioprotectants only potassium hexacyanoferrate(III) seems to be capable of partially mitigating the rate of metal photoreduction at the concentrations used, but not to a sufficient extent that would allow a complete data set to be recorded from a fully oxidized crystal. On the other hand, analysis of the X-ray crystallographic data confirms ascorbate as an efficient protecting agent against radiation damage, other than metal centre reduction, and suggests further testing of HEPES and 2,3-dichloro-1,4-naphthoquinone as potential scavengers.

1. Introduction

Radiation damage to macromolecular crystals is an inherent problem of X-ray crystallography, especially at highly brilliant synchrotron sources (Ravelli & McSweeney, 2000; Gonzalez & Nave, 1994; Garman, 1999; Weik *et al.*, 2000; Burmeister, 2000). The first systematic study on radiation damage in protein crystals was carried out in 1962 at room temperature on myoglobin crystals by Blake and Phillips (Blake & Phillips, 1962). The development and widespread use of cryogenic techniques (Hope, 1988; Garman & Schneider, 1997; Helliwell, 1988) seemed to largely alleviate the problem, since data collection at 100 K usually extends the lifetime of a protein crystal in the X-ray beam by about a factor of 70 (Nave & Garman, 2005; Southworth-Davies *et al.*, 2007) and this was often enough for a complete data set to be collected from a

single crystal. Henderson (1990) predicted, based on electron diffraction experiments, that protein crystals would lose half of their diffracting power at 77 K at an absorbed dose of 20 MGy ($\text{Gy} = \text{J kg}^{-1}$; the Henderson limit). More recent studies based on X-ray diffraction experiments (Owen *et al.*, 2006) suggested a dose of 43 MGy for the same half diffracting power to be reached; they proposed a dose limit of 30 MGy (the Garman limit), above which a macromolecular crystal loses 30% of its initial diffracted intensity and the biological information is compromised. Third-generation synchrotron facilities brought radiation damage back into the spotlight, since such an absorbed dose can nowadays be reached in less than 5 min on the most powerful undulator beamlines.

Mobile reactive species are responsible for specific secondary damage during X-ray irradiation. Their mobility can be partly restrained by data collection at cryogenic

temperatures but solvated electrons are still able to move through the crystal (Jones *et al.*, 1987). While primary damage through direct ionization of protein atoms in the crystal cannot be prevented, secondary damage might be minimized through the addition of scavenger molecules, which intercept the diffusible radicals before they reach the protein.

Changes in diffraction limit and the Wilson B factor are the global indicators traditionally used to recognize radiation damage (Gonzalez & Nave, 1994; Yonath *et al.*, 1998). Most metrics useful as radiation damage monitoring tools [such as R_{sym} , the average $(I)/\sigma(I)$ in the outer resolution shell (Owen *et al.*, 2006), the intensity of a single reflection measured over time] are *post mortem* evidence that radiation damage has occurred and are unsuitable for characterizing onset of damage (Ravelli & McSweeney, 2000). Furthermore, indicators may change over the φ range of data collection for anisotropic crystals (Murray & Garman, 2002), and rates of change might be crystal specific. Specific structural damage has been shown to occur in proteins in a well defined order: breaking or delocalization of disulphide bonds, loss of carboxylate groups from aspartate and glutamate residues (Weik *et al.*, 2000; Burmeister, 2000; Ravelli & McSweeney, 2000; O'Neill *et al.*, 2002; Fioravanti *et al.*, 2007), loss of hydroxyl groups of tyrosines and the methylthio group from methionines. Metal sites seem particularly susceptible to damage (Weik *et al.*, 2000; Dubnovitsky *et al.*, 2005; Colletier *et al.*, 2009) and metalloproteins are partly reduced during X-ray irradiation (Schlichting *et al.*, 2000; Berglund *et al.*, 2002; Adam *et al.*, 2004; Wuerges *et al.*, 2004; Yano *et al.*, 2005; Sato *et al.*, 2004; Beitlich *et al.*, 2007; Corbett *et al.*, 2007; Hough *et al.*, 2008).

At X-ray energies typically used in crystallography, the major cause of radiation damage is the photoelectric effect, which accounts for more than 80% of the interactions with X-rays and matter at 12 keV. The remaining interactions are partitioned roughly equally between inelastic (Compton) and elastic (Rayleigh) scattering (Nave, 1995; Beitlich *et al.*, 2007). The absorption of an X-ray photon results in the ejection of a photoelectron, leaving a hole in the inner shell. This hole is then filled up by an outer-shell electron and concomitant emission of a fluorescence photon or an Auger electron occurs, depending on the binding energy of the electron. In light atoms composing biological macromolecules, the predominant relaxation process is the emission of Auger electrons. This event requires approximately 40 eV, and an average X-ray photon with energy of 13 keV can generate around 300–500 electrons when depositing its energy in the sample (Mozumder & Magee, 1966; Nave, 1995; O'Neill *et al.*, 2002; Beitlich *et al.*, 2007).

Secondary electrons induce further excitation and ionization events within the atoms of the crystal, generating reactive mobile species as well as causing further damage by migrating to the sites of highest electron affinity, in particular metal centres. These are particularly susceptible and have been observed to be reduced very fast, and long before crystalline diffraction is significantly affected (Wuerges *et al.*, 2004; Yano *et al.*, 2005; Schlichting *et al.*, 2000; Berglund *et al.*, 2002; Adam

et al., 2004; Sato *et al.*, 2004; Beitlich *et al.*, 2007; Corbett *et al.*, 2007; Hough *et al.*, 2008). The consequent changes in coordination distances of metal ions upon reduction often do not exceed 0.1 Å (Orpen *et al.*, 1989) and are therefore difficult to discern with X-ray diffraction methods at resolutions typically reachable on crystals of biological macromolecules. Additionally, changes in coordination sphere of metal centres which would occur in solution or at room temperature are reduced in a crystal under cryogenic conditions as movement is reduced (Corbett *et al.*, 2007). Recent studies using X-ray absorption spectroscopy showed that helium-based cooling of crystals to 40 K can notably reduce the metal ion reduction rate (Corbett *et al.*, 2007) and clearly pointed out the need for direct measurement of the redox states of the metals simultaneously with the crystallographic measurements.

Radical scavenging agents are routinely used in fields such as EXAFS (George *et al.*, 1998), electron microscopy (Massover, 2007) or electron spin resonance spectroscopy as spin traps (Jones *et al.*, 1987). Radical scavengers are also known to prevent damage to DNA in solution (Fulford *et al.*, 2001). Zaloga & Sarma (1974) found styrene to be able to extend the lifetime of immunoglobulin crystals tenfold at room temperature and improved resolution. Ascorbate showed encouraging results as a protective agent at 100 K (Murray & Garman, 2002). Evidence that nicotinic acid and 5,5'-dithio-bis-(2-nitrobenzoic acid) (DTNB) can act as free radical scavengers for macromolecular crystallography by quick soaking has been found by Kauffmann *et al.* (2006). A recent thorough screening of potential radioprotectants using cystine and cysteine as models for disulphide bonds and thiol groups, respectively, and monitoring the presence or absence of an absorption peak at 400 nm originating from disulfide radicals (Weik *et al.*, 2002) was performed by Southworth-Davies & Garman (2007). The study confirmed the effectiveness of ascorbate, and suggested reduced dithiothreitol (DTT), quinones and 2,2,6,6-tetramethyl-4-piperidone as further promising candidates.

Characterizing defined oxidation states of metals by means of X-ray crystallography is not trivial. At the resolutions typically reached in macromolecular crystallography, it is intrinsically impossible to detect loss or gain of one electron in electron density maps. Additionally, structural differences between different states are often very subtle. Electrons liberated in the crystal by the incident X-rays during data collection might alter the redox state of the active site and lead to misinterpretations of the resulting data. In fact, many structures published probably represent a mixture of different redox states. For macromolecules with unique UV–Vis absorption spectra sensitive to oxidation state changes, like most metalloproteins, this can be monitored in a straightforward manner by microspectrophotometry (Hadfield & Hajdu, 1993; Bourgeois *et al.*, 2002; Beitlich *et al.*, 2007).

Here we report a systematic study of a wide range of potential soaked-in scavengers to assess their capacity to (i) alleviate photoreduction of metal centres, and (ii) reduce global and specific radiation damage effects in the presence of cryoprotectants and high concentrations of ammonium sulfate

employed here as a common precipitating agent. Two different metalloproteins, horse heart myoglobin and *Pseudomonas aeruginosa* azurin, were studied. Myoglobin is a small heme-containing oxygen storage protein, in which heme iron is bound by a proximal histidine residue and, in the met myoglobin form, a water molecule at the sixth ligand position. Azurin is an electron-transfer protein belonging to a class of blue copper proteins of type 1, where a single copper iron is bound by two histidines, a cysteine, a methionine and a main-chain carbonyl oxygen atom. This coordination sphere can be described as a distorted trigonal bipyramid.

In this study, UV–Vis microspectrophotometry is used to test the efficiency of selected scavengers in decreasing the undesirable photoreduction of iron and copper centres in myoglobin and azurin, respectively. X-ray crystallography was used in parallel to assess their capacity of mitigating global and specific radiation damage effects.

2. Materials and methods

2.1. Potential scavenger selection

Small molecular weight, chemical diversity, solubility and reported scavenger capability were the criteria used for selection of candidate compounds. Potential scavengers screened in this study include several small organic molecules, transition metal complexes and aromatic compounds (see

Fig. 1) including sodium L-ascorbate (SAA), thiourea (TU), 2-nitroimidazole (NI), nicotinic acid (NA), sodium salicylate (NSA), maleic acid anhydride (MA), 4-(2-hydroxyethyl)-1-piperazineethanesulfonic acid [HEPES (HEP)], L-cysteine (CYS), potassium hexacyanoferrate(III) (KF), sodium pentacyanonitrosylferrate(III) (NF), fluorescein (FLU), anthraquinone (AQ), *p*-benzoquinone (BQ), 2,3-dichloro-1,4-naphthoquinone (DNQ), 2,3-dichloro-5,6-dicyano-*p*-benzoquinone (DDQ), 3,4,5,6-tetrachloro-1,2-benzoquinone (TBQ), 5,5'-dithio-bis(2-nitrobenzoic acid) (DTNB) and 2,6-dichloroindophenol (DPI). Chemicals were either bought from Sigma or kindly provided by Walther Schmid from the Institute of Organic Chemistry at the University of Vienna. Although soaking times were kept as short as a few seconds, partial chemical reduction of the azurin metal centre by ascorbate was observed. Two transition metal complexes (NF and KF) were included in the study despite the predicted counteracting effect owing to the large iron X-ray absorption cross section (Murray & Garman, 2002; Southworth-Davies & Garman, 2007).

2.2. Crystallization and soaking

P. aeruginosa azurin (Adman *et al.*, 1978; Nar *et al.*, 1991) and horse heart myoglobin (Sherwood *et al.*, 1987) crystals used in this study were grown under similar conditions to those previously reported. Azurin crystals grow from drops

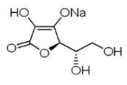
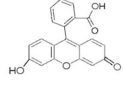
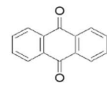
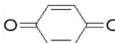
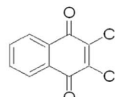
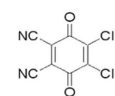
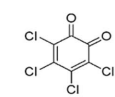
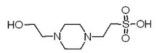
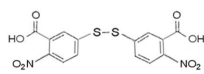
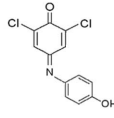
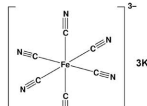
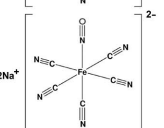
Scavenger		Azurin	Myoglobin	Scavenger		Azurin	Myoglobin		
SAA	Sodium ascorbate		0.2	0.2	FLU	Fluorescein		Saturated	Saturated
TU	Thiourea		0.2	0.2	AQ	Anthraquinone		Saturated	Saturated
NI	2-Nitroimidazole		Saturated	Saturated	BQ	<i>p</i> -Benzoquinone		Saturated	Saturated
NA	Nicotinic acid		0.04	Saturated	DNQ	2,3-Dichloro-1,4-naphthoquinone		Saturated	Saturated
NSA	Sodium salicylate		0.2	0.2	DDQ	2,3-Dichloro-5,6-dicyano- <i>p</i> -benzoquinone		Saturated	Saturated
MA	Maleic acid anhydride		0.1	0.2	TBQ	3,4,5,6-Tetrachloro-1,2-benzoquinone		Saturated	Saturated
HEP	HEPES		0.2	0.2	DTNB	5,5'-Dithio-bis(2-nitrobenzoic acid)		Saturated	Saturated
CYS	L-Cysteine		0.2	0.2	DPI	2,6-Dichloroindophenol		Saturated	Saturated
KF	Potassium hexacyanoferrate(III)		0.1	0.15					
NF	Sodium pentacyanonitrosylferrate(III)		0.2	0.2					

Figure 1

Scavenger formulas and concentrations (*M*) used in soaking myoglobin and azurin crystals for microspectrophotometry and X-ray crystallography experiments.

containing equal amounts of the crystallization cocktail (3.7–3.9 M ammonium sulfate, 1 M lithium nitrate, 10 mM sodium acetate pH 5.8) and protein solution, as large blue plates usually to dimensions of approximately 200 × 150 μm and 10 to 40 μm thick. Rosettes of myoglobin thin red plates grew to variable sizes within a few days from drops set up adding an equal volume of mother liquor (3–3.2 M ammonium sulfate, 100 mM Tris-HCl pH 7.2–7.4 and 4.5% PEG 3350 directly in the drop) to the protein solution. Myoglobin crystals were difficult to reproduce, but addition of PEG 3350 directly to the freshly set up drop improved their quality. Both proteins were crystallized at 295 K, and the proteins were concentrated to 10 mg ml⁻¹. In the case of myoglobin, 5% glycerol was added as cryoprotecting agent by replacing the water in the mother liquor.

Potential scavengers were dissolved directly in the cryoprotecting solution where the crystals were quickly immersed for several seconds (Geremia *et al.*, 2006), before flash-cooling in liquid nitrogen. A concentration of 200 mM was routinely used as described by Kauffmann *et al.* (2006) and Southworth-Davies & Garman (2007), but in some cases (*e.g.* for all quinones tested) the compounds were not soluble at this concentration. Further dilutions of scavengers were necessary in some cases and, when 50 mM was still beyond the solubility limit, experiments were performed with a saturated solution. Dissolving fluorescein in the two cryoprotectants produced very viscous saturated solutions, which were centrifuged several times prior to use. In general, crystals did not show visible signs of degradation during the soaking procedure. Final scavenger concentrations used for soaking azurin and myoglobin crystals for microspectrophotometry and X-ray crystallography experiments are listed in Fig. 1.

Chemically reduced azurin crystals were obtained by soaking in 100 mM β-mercaptoethanol for 1 min. Soaking in 100 mM sodium thiosulfate for 20 h proved to be insufficient to obtain fully reduced myoglobin crystals.

2.3. Dose calculation

The absorbed dose, defined as the energy deposited per unit mass of the crystal, depends on a number of parameters. Composition of the crystal and buffer, crystal size as well as experimental conditions such as the beam energy, flux and dimensions will determine the lifetime of the crystal in the X-ray beam. *RADDOSE*, a program developed by Murray *et al.* (2004), was used to calculate the absorption coefficient of, and hence dose absorbed by, each crystal and define the exposure time needed to reach the aimed absorbed dose (Murray *et al.*, 2005).

Delivered photon fluxes at the crystal position for the data collected on ID14-EH1 and ID14-EH2 at the ESRF were obtained from an online pin diode reading (written out per frame throughout data collection) previously calibrated with a silicon pin diode (S3204-09; Hamamatsu Photonics, Hamamatsu City, Japan) placed directly in the beam. When the number of photons per frame was not available (ID14-EH3, ESRF) the flux was measured with the calibrated silicon pin

diode at the beginning and at the end of each data set and an average was used to calculate the total absorbed dose.

For the X-ray diffraction experiments, special care was taken to match the size of the crystals with respect to the incident beam, to make sure that the entire crystal was smaller than the beam at all times. The target dose was ~8 MGy, which corresponds to 40% of the theoretical Henderson limit and to 27% of the experimental Garman limit. The total absorbed doses were 5.7 MGy for myoglobin and 7.3 MGy for azurin crystals.

2.4. UV–Vis microspectrophotometry experiments

Experiments at the ESRF beamline ID14-EH2 equipped with an online microspectrophotometer allowed the absorption spectrum of the metal centre in the protein crystal kept at 100 K during X-ray exposure to be monitored (McGeehan *et al.*, 2009). The online microspectrophotometer is equipped with a combined deuterium-halogen lamp (DH-2000, Ocean Optics) and a HR4000 spectrophotometer (Ocean Optics). It allows recording of absorption spectra from 250 to 850 nm. The focus of the spectrophotometer (nominal spot diameter of 25 μm) was smaller than that of the X-ray beam (100 × 100 μm), ensuring that only X-ray irradiated material contributes to the recorded spectra.

In UV–Vis microspectrophotometry experiments all crystals were exposed to a dose of about 6.5 MGy (~20 min at the fluxes delivered to the sample; 32.5% of the theoretical Henderson limit and 21.7% of the experimental Garman limit) and their absorption spectrum was monitored throughout the experiment. Owing to beam time limitations one on-line absorption spectrum data set was collected per crystal type in native, chemically reduced and scavenger-soaked states. The orientation of the crystal with respect to the UV–Vis source was optimized to maximize the signal from the metal centre with minimal baseline absorbance. The crystal was kept in this fixed position with respect to the UV–Vis and X-ray beams during irradiation. Ten spectra per second were recorded and averaged in sets of ten to improve the signal-to-noise ratio.

The characteristic features of the spectrum related to the reduction of the metal centre were monitored as a function of time and absorbed dose. Myoglobin and azurin in native, chemically reduced state and native state soaked with the 18 listed scavengers above were used. The changes in the characteristic peak intensities with time (or dose) upon irradiation for both proteins were then fitted to a double exponential equation with offset of the form $A = y_0 + a \exp(-bx) + c \exp(-dx)$, where b and d can be seen as the rate constants describing the fast and slow reduction processes, respectively. Beitlich *et al.* (2007), in a similar study with myoglobin crystals, suggested that d would be the apparent rate constant describing the reduction after the concentration of solvated electrons inside the observed volume has reached a steady state and thus would be the rate constant affected by the effectiveness (or otherwise) of the different scavengers. In the same study, b was thought to be responsible for the initial faster reduction process (~10% of the signal amplitude) and

Table 1

Data collection details for myoglobin and azurin.

All data sets were collected at the ESRF.

Protein	Scavenger	Beamline	Beam size ($\mu\text{m} \times \mu\text{m}$)	Flux (photons s^{-1})	Wavelength (\AA)	Resolution (\AA)	Crystal size ($\mu\text{m} \times \mu\text{m} \times \mu\text{m}$)	Exposure (s)	No. of images	Final dose (MGy)
Azurin	HEP	ID14-3	120 \times 120	7.70×10^{10}	0.931	1.90	0.12 \times 0.1 \times 0.02	3	657	7.30
	Native	ID14-3	120 \times 120	6.47×10^{10}	0.931	1.90	0.1 \times 0.1 \times 0.02	3	782	7.30
	NI	ID14-3	120 \times 120	7.28×10^{10}	0.931	1.90	0.15 \times 0.1 \times 0.02	3	692	7.30
	SAA	ID14-3	120 \times 120	5.58×10^{10}	0.931	1.90	0.1 \times 0.1 \times 0.02	3	900	7.30
	TU	ID14-3	120 \times 120	7.24×10^{10}	0.931	1.90	0.1 \times 0.08 \times 0.02	3	684	7.30
	Native-2	ID14-1	100 \times 100	3.22×10^{10}	0.934	1.80	0.19 \times 0.1 \times 0.01	3	900	7.30
	CYS	ID14-1	120 \times 120	7.10×10^{10}	0.934	1.80	0.12 \times 0.1 \times 0.01	3.5	598	7.30
	DNQ	ID14-1	120 \times 120	5.85×10^{10}	0.934	1.80	0.12 \times 0.1 \times 0.02	3.5	730	7.30
	NA	ID14-1	120 \times 120	5.97×10^{10}	0.934	1.80	0.12 \times 0.08 \times 0.02	3.5	730	7.30
	Myoglobin	Native	ID14-3	100 \times 100	2.59×10^{10}	0.931	1.80	0.16 \times 0.1 \times 0.02	4	841
NSA		ID14-3	120 \times 120	3.94×10^{10}	0.931	1.80	0.1 \times 0.1 \times 0.01	4	900	5.70

considered dependent on the concentration of solvated electrons and the time they take to reach this steady state. It was found that the addition of ascorbate at a concentration between 0.15 and 0.3 M reduced the values of *b* and *d* by 40 and 25%, respectively.

The fitting was carried out using *SigmaPlot* 10.0 (Systat Software Inc, California, USA).

2.5. X-ray data collection and processing

Synchrotron X-ray data were collected from crystals cryo-cooled to 100 K with nitrogen stream using an Oxford Cryo-systems 700 series installed on beamlines ID14-EH1 and ID14-EH3 at the ESRF synchrotron radiation source. X-ray diffraction and online microspectrophotometry experiments were carried out separately using crystals grown under similar conditions. 900° of data were collected for all crystals of both proteins. The number of images used to compose each data set for the subsequent analyses were those necessary to ensure the same total absorbed dose for crystals of the same protein. The data were processed using the *XDS* program package (Kabsch, 1993) and further analysis was carried out using the CCP4 suite of programs (Collaborative Computational Project, Number 4, 1994). Experimental details for all data sets analysed are summarized in Table 1.

Each data set was divided into five subsets with increasing dose, which were subsequently indexed and integrated individually. Several of the myoglobin subsets had to be reindexed using *POINTLESS* (Evans, 2006) and *REINDEX* (Collaborative Computational Project, Number 4, 1994), to ensure consistency within each series. The subsets within one series were scaled together using *XSCALE* (Kabsch, 1993) and were assigned the same test set of reflections. Data collection statistics for azurin and myoglobin subsets 1 (low dose) and 5 (high dose) are shown in Tables 2 and 3. R_{free} was calculated based on 5% of reflections excluded from the refinement.

2.6. Structure solution and refinement

Structures were solved by molecular replacement using *MOLREP* (Vagin & Teplyakov, 1997) using available structures with access codes 4AZU (Nar *et al.*, 1991) and 1WLA

(Maurus *et al.*, 1997) as search models for azurin and myoglobin, respectively. In some cases molecular replacement could be avoided and the starting model directly refined against the X-ray data. Solvent molecules and metal ions were removed from the starting search model and a small random kick of 0.3 Å was applied to all atoms using *PDBSET* (Collaborative Computational Project, Number 4, 1994) to reduce model bias.

The model was refined against the low dose (first) subset of each series only. Refinement was carried out using the maximum likelihood functions implemented in *REFMAC5* (Murshudov *et al.*, 1997). Rounds of ten cycles of restrained refinement were alternated with manual inspection of the electron density maps and model building with *COOT* (Emsley & Cowtan, 2004). Calculated phases were subsequently used for generating $|F_{\text{ox}}| - |F_{\text{ol}}|$ ($x = 2, 3, 4, 5$) difference maps, and local specific damage effects were analysed on the basis of peak heights. Water molecules were added using *ARP/wARP* (Perrakis *et al.*, 1999), and were subsequently excluded from the final model if their *B* factor exceeded two times the Wilson *B* factor and the electron density was not well defined. Refinement statistics for azurin and myoglobin data sets are shown in Tables 2 and 3, respectively.

3. Results and discussion

3.1. UV–Vis microspectrophotometry

Spectra with well defined characteristics were collected for azurin and myoglobin. Their spectral features change markedly upon reduction (Dennison, 2005) and the plate-shaped crystals obtained for both proteins are ideal for this technique, as orientation of the specimen with the shortest dimension perpendicular to the beam allows minimization of optical absorption. In more cube-like crystals, absorption may become too high owing to the long path length and render these experiments impossible.

In an attempt to quantify the relative contribution of the scavenger to the spectral changes upon irradiation, spectra of candidate scavengers dissolved in azurin cryoprotecting solution at 100 K were also measured. Azurin crystals are typically

radiation damage

Table 2

Data collection and refinement statistics for azurin.

Each data set was divided into five subsets, each of which corresponds to an absorbed dose of 1.46 MGy. Set 1 is the lowest dose subset and Set 5 the highest. Values in parentheses are for the outer resolution shell.

	Native		Native-2		HEP		NI		SAA	
	Set 1	Set 5								
Resolution limits (Å)	50–1.9 (2.17–1.9)									
Unit-cell parameters										
<i>a</i> (Å)	56.87	56.89	56.98	57.08	56.75	56.78	56.85	56.90	56.67	56.77
<i>b</i> (Å)	80.01	80.01	80.15	80.32	79.78	79.81	79.64	79.70	79.43	79.55
<i>c</i> (Å)	109.56	109.58	109.77	110.02	109.57	109.69	109.23	109.40	109.31	109.52
Mosaicity (°)	0.20	0.20	0.25	0.26	0.11	0.11	0.13	0.10	0.15	0.13
Total No. of reflections	255452	253229	288559	287327	207765	208273	217393	219080	283946	281689
No. of unique reflections	40481	40466	39985	39812	39441	39466	39345	38940	38310	38180
Completeness (%)	98.2 (96.1)	98.1 (96.2)	98.7 (97.4)	98.2 (96.6)	98.5 (97.6)	98.6 (97.4)	98.7 (97.6)	97.7 (96.4)	96.4 (94.6)	96.1 (94.1)
<i>I</i> / σ (<i>I</i>)	14.7 (4.9)	15.3 (4.9)	16.7 (6.5)	15.1 (5.2)	14.3 (8.3)	13.4 (7.3)	16.5 (9.2)	12.9 (6.6)	14.3 (6.7)	14.1 (6.4)
<i>R</i> _{meas} (%)†	10.3 (41.8)	10.2 (41.9)	9.8 (32.7)	11.7 (41.9)	8.8 (20.3)	9.6 (23.8)	7.7 (18.6)	10.5 (29.1)	10.9 (31.6)	11.3 (33.3)
Wilson <i>B</i> (Å ²)	23.7	25.4	21.9	23.5	20.5	22.0	21.3	22.1	22.2	23.3
<i>R</i> (%)‡	18.3		17.8		17.1		17.7		17.5	
<i>R</i> _{free} (%)‡	23.6		22.5		21.8		21.5		21.8	
RMS bond (Å)	0.018		0.015		0.014		0.015		0.014	
RMS angle (°)	1.5		1.5		1.4		1.4		1.5	

	TU		CYS		DNQ		NA	
	Set 1	Set 5						
Resolution limits (Å)	50–1.9 (2.17–1.9)							
Unit-cell parameters								
<i>a</i> (Å)	56.53	56.68	56.97	57.06	57.01	57.08	57.09	57.12
<i>b</i> (Å)	79.91	80.11	80.00	80.15	80.16	80.33	80.11	80.11
<i>c</i> (Å)	109.72	110.05	109.18	109.42	109.46	109.65	109.54	109.67
Mosaicity (°)	0.24	0.25	0.20	0.22	0.42	0.39	0.52	0.50
Total No. reflections	214793	215783	181744	182461	230224	230044	218222	218474
No. of unique reflections	39232	39109	38990	36499	39771	39783	39650	39747
Completeness (%)	97.9 (95.4)	97.6 (95.1)	97.0 (95.6)	90.8 (91.3)	98.5 (97.6)	98.5 (97.9)	98 (96.9)	98.3 (96.9)
<i>I</i> / σ (<i>I</i>)	13.1 (5.9)	11.9 (4.8)	18.0 (6.8)	16.4 (5.8)	13.6 (4.5)	13.9 (4.2)	11.2 (3.9)	10.0 (3.3)
<i>R</i> _{meas} (%)†	10.2 (30.6)	11.9 (38.4)	6.8 (23.5)	7.8 (29.0)	10 (41.6)	10.6 (45.6)	12.7 (45.1)	14.8 (54.0)
Wilson <i>B</i> (Å ²)	21.1	22.9	24.8	25.5	26.2	27.6	24.7	25.7
<i>R</i> (%)‡	18.2		19		18.8		19.1	
<i>R</i> _{free} (%)‡	22.7		23.8		23.7		25.6	
RMS bond (Å)	0.016		0.017		0.017		0.018	
RMS angle (°)	1.6		1.6		1.7		1.8	

† $R_{\text{meas}} = \sum_h (n_h/n_h - 1) \sum_i |I(h,i) - \langle I(h) \rangle| / \sum_h \sum_i I(h,i)$, where $I(h,i)$ is the intensity of the i th measurement of reflection h and $\langle I(h) \rangle$ is the mean value of $I(h,i)$ for all i measurements and n_h is the number of observations of reflection h . ‡ $R = \sum_{hkl} |F_o| - |F_c| / \sum |F_o|$, where F_o is the observed structure factor amplitude and F_c the calculated structure-factor amplitude. R_{free} is calculated based on 5% of reflections not used in refinement.

reduced after a 2 h soak in a solution containing 10 mM ascorbate (Li *et al.*, 2006). In this study, samples soaked in 0.2 M ascorbate for a few seconds did show partial reduction but further photoreduction could be observed during the course of X-ray exposure.

3.1.1. Azurin. The spectrum of azurin shows a broad peak around 632 nm owing to a S(Cys) → Cu(II) ligand-to-metal charge transfer transition that is not present when the copper is reduced. The decrease in absorbance of this band was followed during the course of X-ray exposure and is depicted in Fig. 2 with increasing doses for (a) native (b) TU, (e) KF and (g) ascorbate soaked crystals. For most samples the loss of this

peak (copper reduction) is a two-step process: fast at the beginning of the exposure and then slowing down over time/dose.

In all spectra we observe an isosbestic point which indicates that the reactant and product are two absorbing species (absorbing at 632 nm and below 500 nm, respectively) in equilibrium without the formation of an intermediate. The only exceptions observed were the spectra of NF-soaked crystals, where generation of a novel species forming at high doses with absorption in the 400–600 nm range alters the spectra and masks the identification of the isosbestic point. These data were therefore not analysed further.

Table 3

Data collection and refinement statistics for myoglobin.

Each data set was divided into five subsets, each of which corresponds to an absorbed dose of 1.14 MGy. Set 1 is the lowest dose subset and Set 5 the highest.

	Native		NSA	
	Set 1	Set 5	Set 1	Set 5
Resolution limits (Å)	50–1.8 (2.10–1.8)	50–1.8 (2.10–1.8)	50–1.8 (2.10–1.8)	50–1.8 (2.10–1.8)
Unit-cell parameters				
<i>a</i> (Å)	35.23	34.96	35.27	35.28
<i>b</i> (Å)	28.64	28.46	28.55	28.55
<i>c</i> (Å)	62.90	62.64	62.87	62.90
β (°)	106.1	106.4	105.8	105.8
Mosaicity (°)	0.65	0.66	0.22	0.24
Total No. of reflections	37011	37644	40364	40109
No. of unique reflections	11196	11232	11237	11225
Completeness (%)	97.5 (95.7)	97.8 (96.9)	98.0 (96.8)	97.9 (96.6)
<i>I</i> / σ (<i>I</i>)	12.4 (5.0)	11.7 (5.1)	19.0 (9.7)	21.0 (11.9)
<i>R</i> _{meas} (%)†	7.7 (28.3)	7.9 (26.7)	5.6 (14.1)	5.0 (11.5)
Wilson <i>B</i> (Å ²)	26.0	25.2	22.7	23.0
<i>R</i> (%) §	16.7		16.2	
<i>R</i> _{free} (%)‡	24.0		21.4	
RMS bond (Å)	0.017		0.012	
RMS angle (°)	1.6		1.2	

† $R_{\text{meas}} = \sum_i (n_i/n_h - 1) \sum_j |I(h,i) - \langle I(h) \rangle| / \sum_i \sum_j I(h,i)$, where $I(h,i)$ is the intensity of the *i*th measurement of reflection *h* and $\langle I(h) \rangle$ is the mean value of $I(h,i)$ for all *i* measurements and n_h is the number of observations of reflection *h*. ‡ $R = \sum_{hkl} |F_o| - |F_c| / \sum |F_o|$, where F_o is the observed structure factor amplitude and F_c the calculated structure-factor amplitude. R_{free} is calculated based on 5% of reflections not used in refinement.

Solvated electrons are visible immediately upon irradiation owing to a pronounced peak appearing at around 600 nm that will decay with time as observed for myoglobin and reduced DTT in solution (Southworth-Davies & Garman, 2007; Beitlich *et al.*, 2007). In the spectra of azurin, the solvated electron signature peak, which would interfere with the 632 nm peak, is not observed. This was confirmed in the control experiments where spectra of cryosolution plus scavengers alone (no crystals) were exposed to increasing X-ray doses and Fig. 3 shows the spectra measured from KF. No changes are visible after an absorbed dose of 1.2 MGy at around 600 nm (from the signature peak of solvated electrons).

Peak decrease. The scaling of spectra was performed, and the absorbance at 760 nm was chosen as baseline absorbance and subtracted from the absorbance around 630 nm. Assuming that crystals are fully oxidized at the beginning of the experiment and that the solution around the crystal adds a constant contribution throughout the relevant wavelength range, the difference between $\text{Abs}_{760\text{nm}}$ and $\text{Abs}_{632\text{nm}}$ was taken as a 100% peak. The decrease of the peak after absorption of a dose of around 6.5 MGy can then be determined for each scavenger-soaked sample. This procedure is consistent with the observation that in a chemically reduced crystal the characteristic peak at 632 nm is not observed (see Fig. 2), but does not take into account a possible initial reduction by ascorbate prior to X-ray irradiation.

Peak height decrease in percentage for all the azurin samples is shown in Fig. 4(a). The Cu(II) peak at 632 nm does not disappear completely for any of the samples. Comparison with the spectrum collected from a chemically reduced azurin crystal (soaked in 100 mM β -mercaptoethanol for 1 min) shows that complete X-ray-induced photoreduction does not occur at the doses absorbed (see Fig. 2). The decrease of the Cu(II) peak caused by the photoreduction is smaller than that observed for the native crystals only in the case of the transition metal complex KF (Fig. 4a), while the spectra of NF-soaked azurin showed the generation of a new species with absorption in the 400–600 nm region, preventing a reliable extraction of the peak decrease. This suggests that, from the tested compounds, only KF is able to alleviate the undesirable effect of metal reduction in the X-ray beam.

Rate constants. The fit of the decrease of the characteristic peak at 632 nm of Cu(II) azurin with increasing dose to the double exponential function with offset described in §2.5 can be achieved for all scavengers except NF. The quality of the fit was very high for all samples, as assessed both by $R^2 > 0.91$ and by the probability $p < 0.0001$ calculated for the coefficients. The ‘rate constants’ *b* and *d* are characteristic for the shape of the time course curves and their fit values were the same for raw and scaled data. Figs. 2(b), 2(d), 2(f) and 2(h) show the time course of the 632 nm peak during X-ray exposure measured from a native, TU, KF and SAA soaked azurin crystal, respectively. Fig. 4(b) depicts the rate constants *b* and *d* for the decay of the 632 nm peak for all azurin samples. The results on native azurin crystals show an outlier which we cannot explain and attributed it to a systematic experimental error during acquisition of data, which we do not know the cause of. For the sake of the correct reporting of experimental results we kept these data in the manuscript.

The larger rate constant, *b* describes how fast the initial reduction occurs. The results in Fig. 4(b) show that adding most of the tested scavengers decreases *d*, but not necessarily *b*. Using the average of the native crystals as a reference, the most significant reduction of *b* was observed for KF (86%), DNQ (37.5%) and BQ (35.8%). Somewhat stronger effects can be seen for the rate constant *d*, with the scavenger compounds HEP, SAA, KF, NSA and TU (all with a reduction percentage above 90%) being the best candidates. Combination of the results on two rate constants *b* and *d* suggests KF, NSA and DNQ as having the stronger effects on avoiding the decay of azurin’s 632 nm copper peak during X-ray-induced photoreduction. It is to be noted that SAA yields an increase in *b* of above 100%.

The initial fast reduction of azurin accounts for up to 71% (SAA) of the total signal amplitudes. The scavengers for which this initial fast reduction process made up a bigger proportion of the total signal amplitudes observed are SAA (71%), DNQ (62%), HEP (56%) and NSA (56%), a shortlist that carries a strong resemblance to that obtained from the rate constant analysis. Excluding the special case of KF, where no initial fast reduction process can be seen, the weight of the initial fast reduction process is lowest for the native crystal. Addition of scavengers has some effect in the slower step of photoreduc-

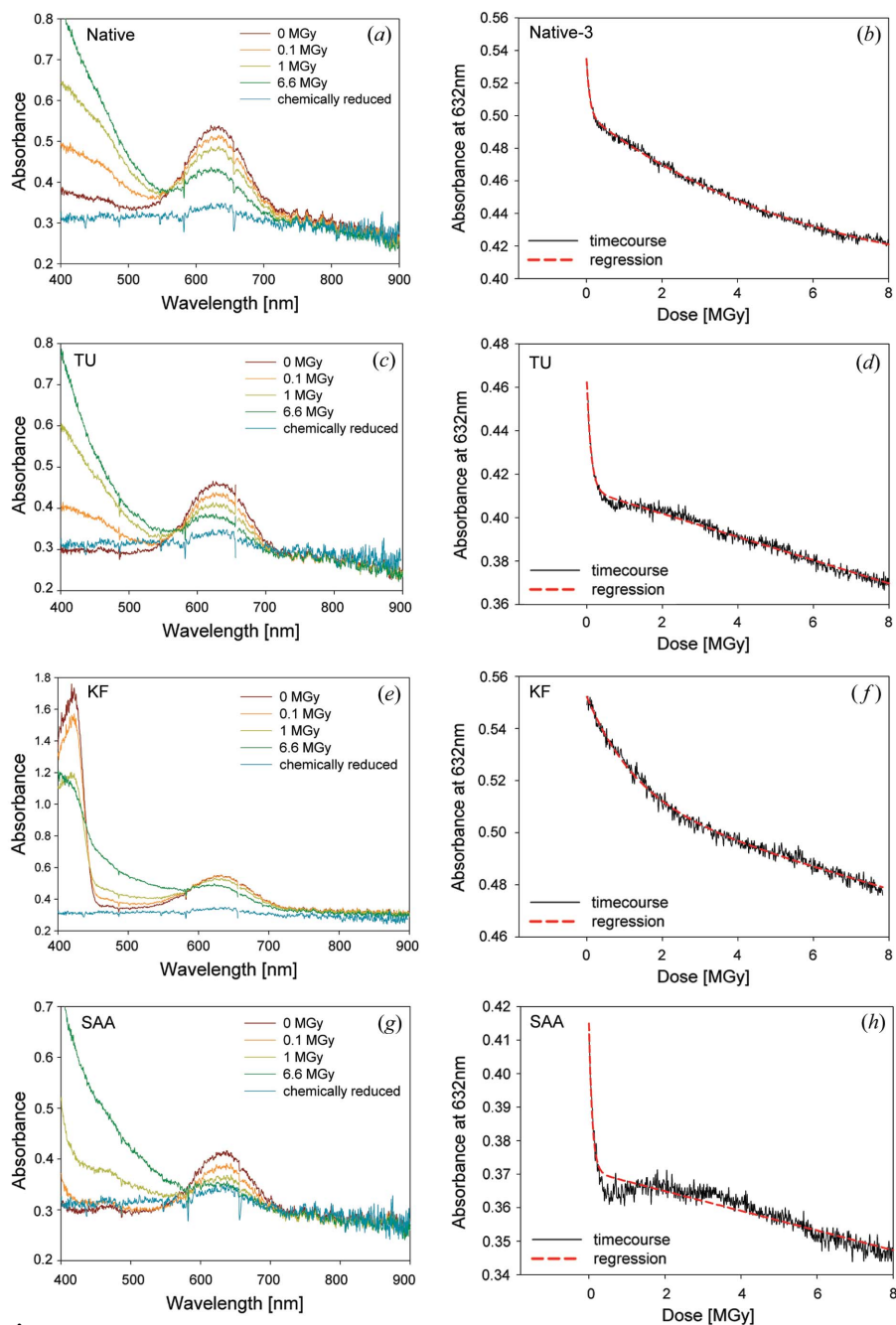


Figure 2 Spectra measured from (a) native, (c) TU, (e) KF and (g) SAA soaked azurin crystals with increasing dose. The total dose absorbed by the crystals was around 6.5 MGy. Time course curves at 632 nm during irradiation for (b) native and (d) TU, (f) KF and (h) SAA soaked azurin with fits to the double exponential function with offset.

tion. The dose at the turnover between fast and slow reduction processes (defined as the rough dose estimate at the point of change in slope) is around 0.4 MGy for most spectra measured, independent of whether it is a native or a scavenger soaked sample. If one can expect a clear loss of signal amplitudes above 50% after an absorbed dose of only 0.4 MGy, it seems improbable that these scavenger compounds can avoid X-ray-induced photoreduction of the copper in the active site of azurin during diffraction data collection. On the other hand, KF seems to be able to at least

partially delay metal reduction, but quantification of the degree of its efficiency requires further studies.

3.1.2. Myoglobin. The spectrum of Met myoglobin (ferric, Fe^{3+} myoglobin that has a water molecule bound at the sixth ligand position of the haem iron) is more complex than that of Cu(II) azurin, and the strong characteristic features appear upon reduction of Fe^{3+} to Fe^{2+} . This can be seen in Fig. 5, where the spectral changes monitored with increasing dose to (a) native and (c) TU, (e) KF and (g) SAA soaked crystals are shown. According to Beitlich *et al.* (2007), one should expect a shift of the Soret band from 413 nm to 427 nm, two new double peaks at 528/536 and 555/566 nm and a slow decrease of the bands between 500 and 700 nm upon reduction. With the experimental set-up and crystals used in this study, the shift of the Soret band could be observed only in a few cases. The two double peaks, on the other hand, can be distinguished well in most of the spectra. Following the procedure used by Beitlich *et al.* (2007), absorbances at 555 nm were subtracted from those measured at 566 nm in order to eliminate possible interference in absorbance by solvated electrons, which were present in the case of myoglobin but not azurin. Time course absorbance changes in the spectra were monitored during exposure to X-rays.

Rate constants. The time course curves of the increase of the 566–555 nm absorbances in myoglobin spectra were also fitted to a double exponential function with an offset, as used for azurin. Time course curves for one native crystal and crystals soaked in AQ, HEP, MA, SAA and TU (see Fig. 4c) gave acceptable fits and were used to calculate rate constants b and d .

The rate constants for the scavenger-soaked crystals are given as a percentage of the value obtained for the native crystal. The samples presenting a fit with $R^2 < 0.7$ or those for which the coefficients of the double exponential could not be estimated well ($p > 0.0001$) were disregarded. Different shapes for the time course curves were observed, some of which were clearly flat and could not yield a good quality fit with the double exponential function. The different shapes seem to result from spectral changes that do not stem from the reduction of the metal centre. In the case of myoglobin, none of the values obtained for the scavenger-

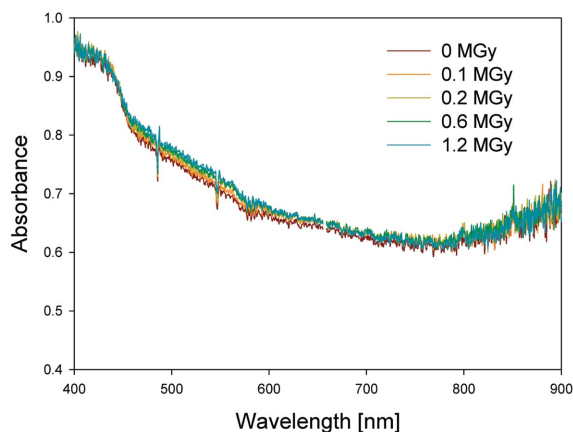


Figure 3
Spectra measured from KF dissolved in the azurin cryosolution alone (no crystal) with increasing dose. The total dose absorbed was 1.2 MGy.

soaked crystals represent a decrease in the rate constants as related to the average of the native crystal, suggesting that addition of these five scavengers does not slow down reduction of the metal centre of the protein. Further testing is necessary to assess the effectiveness of the remainder of the scavengers included in this study.

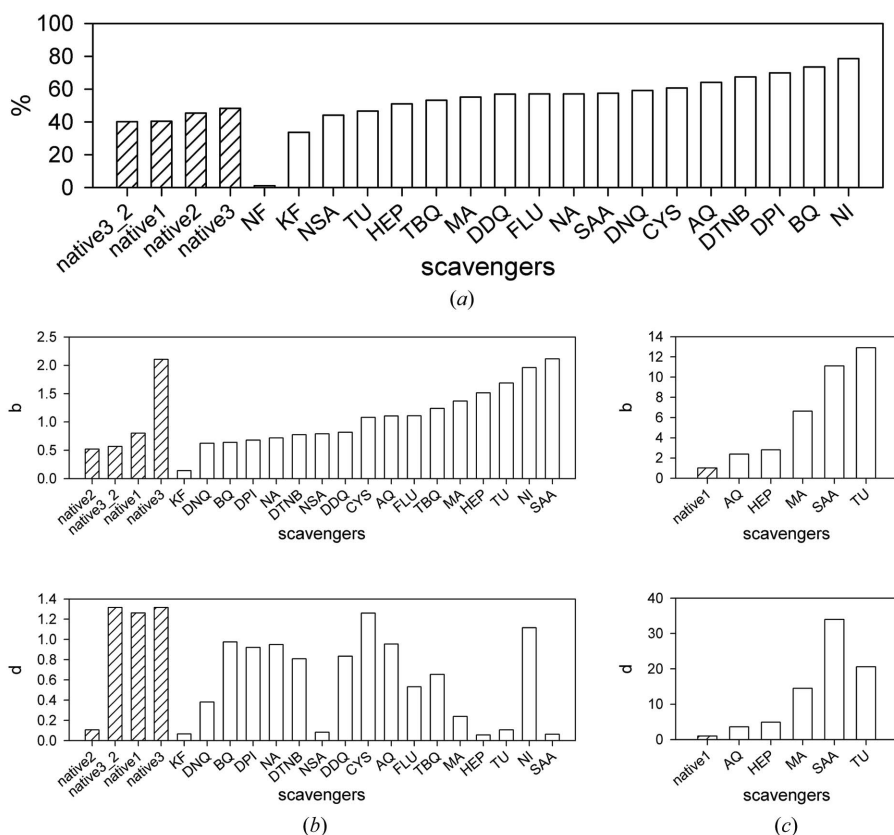


Figure 4
Decrease in percentage absorbance of the 632 nm peak of Cu(II) azurin after absorption of a dose around 6.5 MGy assuming that samples are (a) fully oxidized at the beginning of the experiment; (b) rate constants b and d as calculated for a fit of double exponential with offset for azurin and (c) myoglobin samples. The rate constants b and d shown in the graphs are relative to the average of the native crystal(s). In the case of myoglobin, only crystals for which the quality of fit is good ($R^2 > 0.7$ and $p < 0.0001$ for the coefficients calculated) were included.

The initial fast reduction accounts for 100% (SAA) to 44% (native) of the total signal amplitudes for myoglobin. The fact that the fast process is less important for the native sample is consistent with what was observed for most azurin-soaked samples, and indicates that soaking with scavengers only affects the slower reduction process. The dose at the turnover between fast and slow reduction process is, unlike what was observed for azurin, higher (1.5 MGy) for the native crystals. Most of the metal centre reduction occurs in the initial fast process and addition of radioprotectant compounds seems to lower the dose at which the turnover takes place (as low as 0.6 MGy in the case of SAA).

Transition metal complex as scavengers. It has been suggested that transition metal complexes could act as potentially active radioprotectants in protein crystals (Jones *et al.*, 1987). In the specific case of KF the electron would be preferentially transferred to an Fe atom, which would then suffer reduction and prevent local damage in the metal centre of the protein (Burmeister, 2000). However, the presence of such metal ions at the concentrations necessary significantly increases the dose absorbed by the sample and reduces to half the exposure time needed to reach the Henderson limit at a wavelength of 0.94 Å (Murray & Garman, 2002; Southworth-Davies & Garman, 2007).

This means that only highly efficient metal-containing radioprotectants would be able to outweigh the deleterious effects of the increased absorption cross section and/or act as an oxidizing agents in the case of some metalloenzymes, depending on the redox potential of the metal centres [$E^0(\text{Fe}^{3+}/\text{Fe}^{2+})$ in KF = 0.420 eV; $E^0(\text{Cu}^{2+}/\text{Cu}^{1+})$ in azurin = 0.340 eV and pH = 5.8; $E^0(\text{Fe}^{3+}/\text{Fe}^{2+})$ in myoglobin = 0.0589 eV (O'Reilly, 1973; Yanagisawa & Dennison, 2004; Varadarajan *et al.*, 1989)].

Based on the fitted b and d rate constants alone, KF seems to be a promising scavenger in preventing X-ray-induced photoreduction in the case of azurin. The peak decrease percentages calculated for azurin at 632 nm (assuming fully oxidized samples at the beginning of the experiments) suggests some effect of KF in mitigating photoreduction during exposure to X-rays. The spectra of the cryoprotecting solutions alone (containing KF) at increasing doses show that absorbance and spectral characteristics in general are not dose dependent, indicating that the scavenger does not interfere with the measurements at the wavelengths monitored.

radiation damage

The fit of amplitude decay for the KF-soaked crystal can be described by rate constant d alone, since the contribution of b is negligible. Using only d as metric, the scavengers KF, NSA, HEP, TU and SAA seem the most promising, which is in line with the observations of scavenger efficiency through crystallographic data analysis exposed below.

3.2. X-ray crystallography

Nine azurin data sets were collected, two from native crystals and the remaining from crystals soaked in HEP, NI, SAA, TU, CYS, DNQ and NA. Crystals belonged to space group $P2_12_12_1$ with unit-cell dimensions of $a = 57.00 \text{ \AA}$, $b = 80.00 \text{ \AA}$, $c = 109.50 \text{ \AA}$ and four molecules in the asymmetric unit. The resolution cut-off chosen for all azurin data sets was 1.9 \AA .

Two data sets collected from myoglobin crystals have been included in this analysis, one from a native crystal and one from a crystal soaked in NSA. Myoglobin crystals belonged to space group $P2_1$, with unit-cell dimensions of $a = 35.00 \text{ \AA}$, $b = 28.50 \text{ \AA}$, $c = 62.90 \text{ \AA}$, $\beta = 106.0^\circ$ and a single molecule in the asymmetric unit. The resolution cut-off used was 1.8 \AA .

Each complete data set was divided into five subsets (referred to as subsets 1 to 5, 1 being the one with lower dose), and each subset was integrated separately. Statistics are displayed in Table 2 for azurin data sets and in Table 3 for myoglobin data sets.

3.2.1. Radiation damage indicators with increasing dose. The relatively weak lattice contacts in protein crystals are easily disrupted by radiolytic products resulting from absorbed photons, making them particularly prone to radiation damage (Gonzalez & Nave, 1994; Murray *et al.*, 2005). General radiation damage indicators such as unit-cell volumes, R_{meas} , $I/\sigma(I)$, completeness in the highest-resolution shell and Wilson B factors for each subset were monitored and compared. The evolution of unit-cell volume (\AA^3), R_{meas} (%) and Wilson B factor (\AA^2) with increasing dose is depicted in Fig. 6. Wilson B factor values used for this comparison were taken from each subset when scaled separately, while the remaining statistics were obtained after scaling against the low dose subset. Analysis in this section refers to azurin.

The overall Wilson B factors show a close-to-linear increase with absorbed dose (see Fig. 6a). SAA and DNQ show the

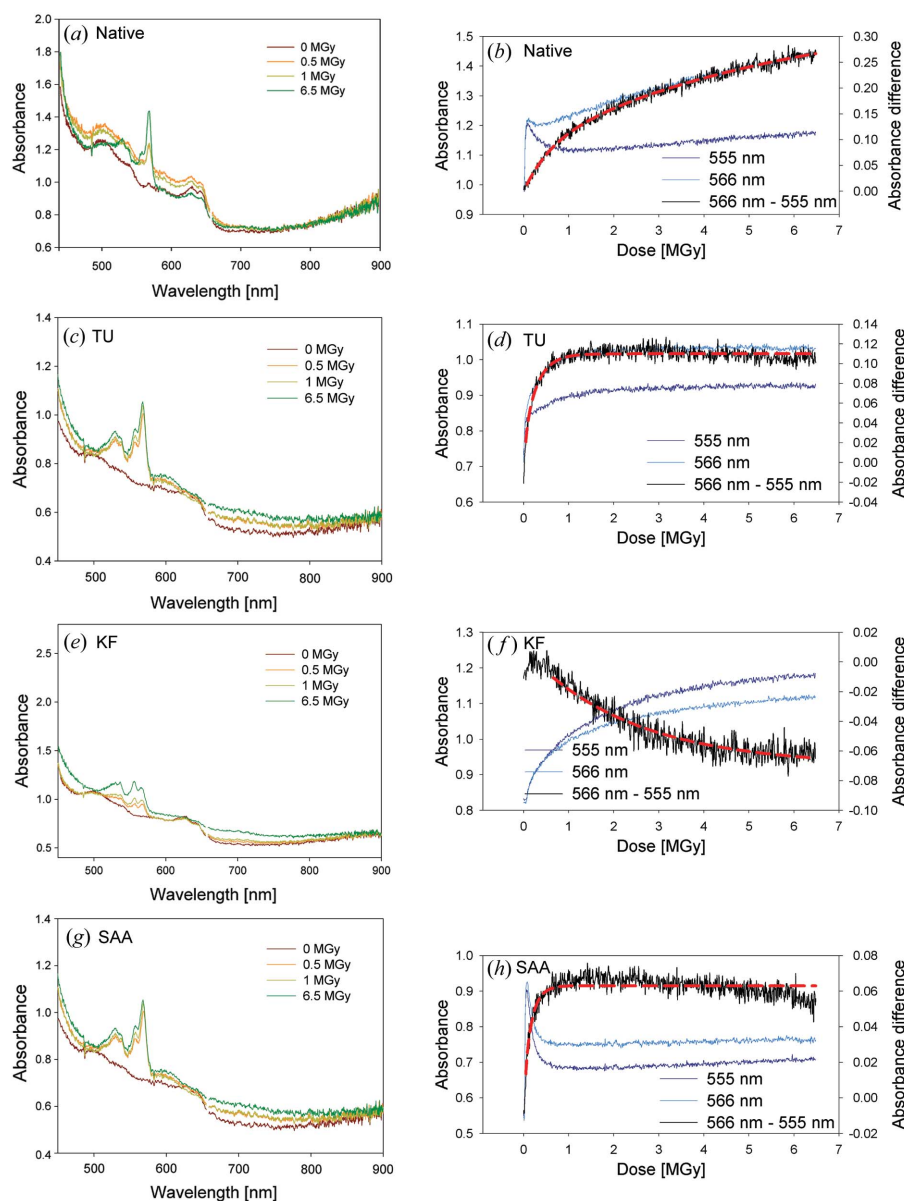


Figure 5

Spectra measured from (a) native and (c) TU, (e) KF and (g) SAA soaked myoglobin crystals with increasing dose. The total dose absorbed by the crystals was around 6.5 MGy. Different shapes were observed for the time course curves of the peak at 566 nm: (b) native and (d) TU, (f) KF and (h) SAA soaked crystals with fits to the double exponential function with offset. The absorbance at 555 nm was subtracted from that at 566 nm to try to minimize the effects of solvated electrons.

slowest rise of Wilson B factor. A general upwards trend can be observed for the evolution of R_{meas} with increasing dose in most of the data sets (see Fig. 6b), but fluctuations in the trends can be observed. SAA and HEP are the data sets displaying the least fluctuations and the smallest increase of R_{meas} over all subsets. Unit-cell volumes (see Fig. 6c) and completeness in the last resolution shell (Table 2) exhibit small changes from one subset to the next, while we observe consistent decrease of $I/\sigma(I)$ with increasing dose (Table 2). From the global indicators used in this study, the evolution of Wilson B factors, R_{meas} and $I/\sigma(I)$ seems to be sensitive enough and therefore indicative of radiation damage. Completeness in the last resolution shell displays a small

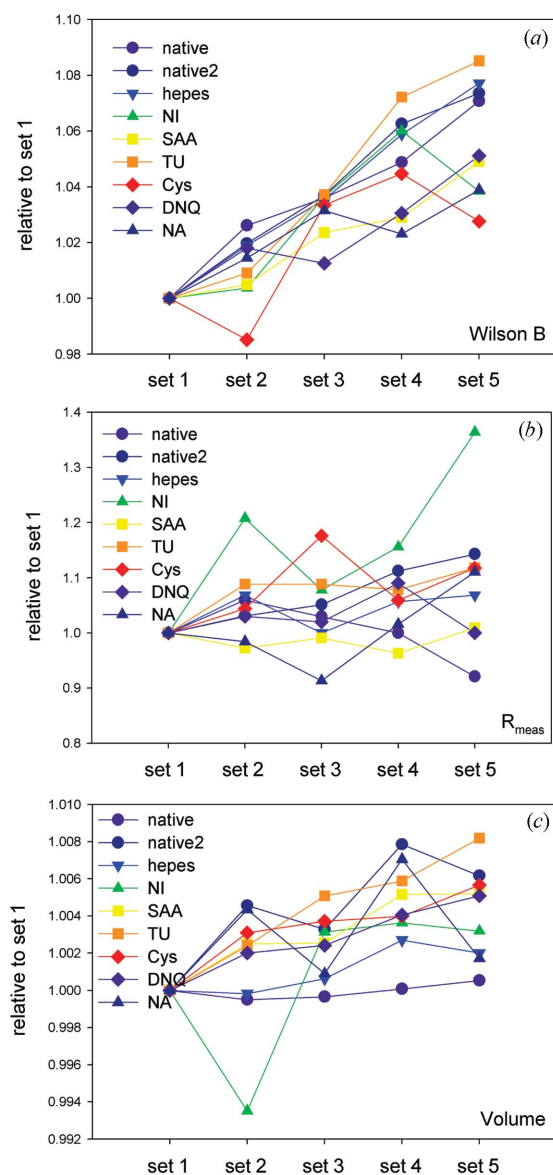


Figure 6
 (a) Wilson B factor, (b) R_{meas} and (c) unit-cell volume as they evolve over the five subsets for data collected from the nine measured azurin crystals. The total absorbed dose per data set was 7.3 MGy, and each subset corresponds to a fifth of that dose. Values are relative to the lowest dose subset (Set 1).

decrease when the first and the last subsets are compared, while the unit-cell volume and mosaicity (data not shown) changes are small and/or the trends are unclear or unstable, probably affected by highly anisotropic crystals (Murray & Garman, 2002).

3.2.2. R_d plots. Sliz *et al.* (2003) introduced the calculation of a merging R -factor between reflections occurring in the first image of a data set and those of subsequent images. The ‘decay R -factor’ proposed by Diederichs (2006) is a simple quantitative way to assess radiation damage based on the measured data, without the need to scale it or choose a theoretical radiation damage model. A plot of fractional differences is calculated by analogy to the usual R -factor as a function of the

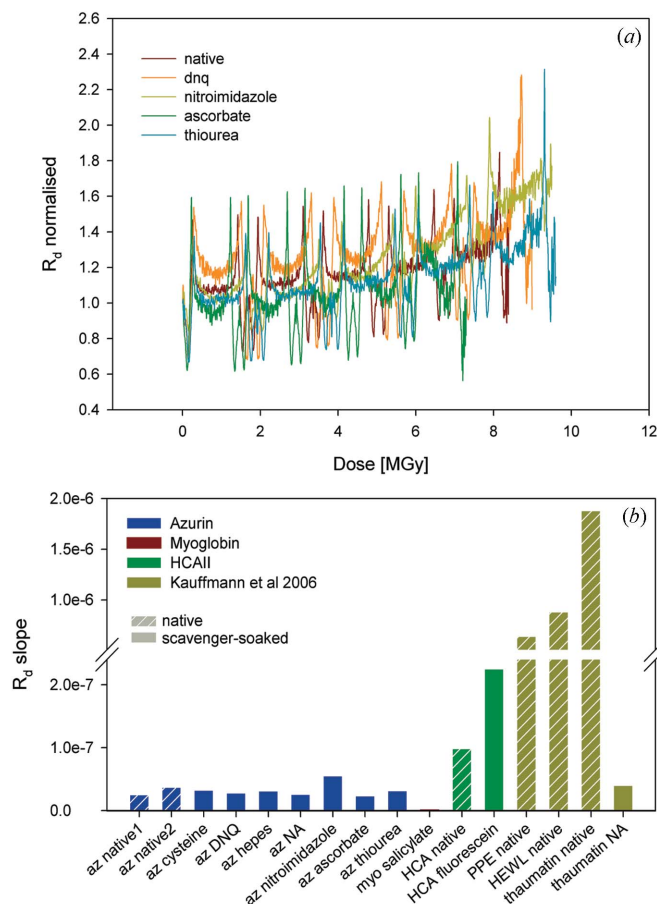


Figure 7
 R_d plots calculated for some of the azurin data sets (a) and R_d slopes as calculated for all data sets included in this study as well as those found in other studies (b). R_d values have been normalized to allow direct comparison between different crystals.

separation of the contributing observations in frame number (and dose). A positive slope in the linear fit indicates significant radiation damage. As in the study by Kauffmann *et al.* (2006), R_d plots were used in an attempt to quantify the relative efficiency of each scavenger using data from a native crystal as reference. The plots have been calculated for all the data sets using *XDSSTAT* (Diederichs, 2006). The program outputs an R_d value for each frame difference (*i.e.* for all pairs of reflections on frame i and j , where the frame difference $d = |i - j|$). The number of frames contributing to each value is very small for the largest frame differences and therefore the linear fit was weighted by the number of frames. The relative slopes were calculated and compared. Plots for some of the azurin data sets are shown in Fig. 7(a). Fitting and further statistical analysis were performed using the program *Sigma-plot* (Systat Software).

Fig. 7(b) shows the magnitude of the slopes for all data sets analysed in this study along with those obtained for native human carbonic anhydrase II and a crystal soaked in fluorescein (HCAII, data kindly provided by Björn Sjöblom from the Department for Biomolecular Structural Chemistry of the University of Vienna). For comparison, slopes observed by Kauffmann *et al.* (2006) have also been included. The differ-

ences are striking, with the slope values obtained by Kauffmann *et al.* being one to two orders of magnitude bigger than those calculated for the myoglobin and azurin samples in this study. Given that the experimental procedure was very similar in the two cases, and that the absorbed doses are considerably higher in our case, this observation is particularly surprising and suggestive of a radiation protective effect of the high concentration of ammonium sulfate (3.8 and 3.2 M, respectively), which is the precipitating agent used for both azurin and myoglobin. In the presence of high concentrations of SO_4^{2-} ions, a large amount of $\text{SO}_4^{\bullet 2-}$ radical forms in the solvent (Burmeister, 2000; Beitlich *et al.*, 2007). This radical is a strong electron acceptor (von Sonntag & Schuchmann, 1994) and can function as a scavenger. This is consistent with spectroscopic evidence that azurin crystals are not fully reduced in the X-ray beam at the end of the experiments, but the same does not seem to be the case for myoglobin. No spectra could be measured from a chemically reduced myoglobin crystal since reduction under the conditions used (soaked in 100 mM sodium thiosulfate for 20 h) proved to be incomplete. Additionally, structure analysis of models shows limited specific local structural damage caused to azurin after a dose of 7.3 MGy.

The surprisingly low slopes obtained together with the low correlation coefficients make the selection of the efficient scavengers based on R_d slopes very difficult. There are only a few cases in which the differences between a native data set and one including a scavenger are bigger than those observed between two native data sets of the same protein. Within the experience obtained so far, the slopes of R_d appear to be reproducible across data sets from crystals of the same drop (Diederichs, 2006). Owing to the large number of crystals employed in this study, it was impossible to ensure that samples from each protein were harvested from the same drop. For the proteins studied and the doses applied here, the slope of the R_d plot does not seem to be comparable between different proteins and could not be used efficiently to select useful scavengers for macromolecular crystallography.

3.2.3. Local specific damage analysis. To investigate the local specific damage, difference $|F_o| - |F_c|$ maps were calculated using the calculated phases obtained from the refined model of the lower dose subset. The coordinates of all peaks higher than the 3σ level were sorted and assigned to specific parts of the structure to allow evaluation of local structural changes. Average peak heights close to the most susceptible residues were then calculated for each pair of data subsets. Peak heights in scavenger-soaked crystals were compared with those of the native samples for the assessment of scavenger effectiveness.

In azurin the most affected groups are the carboxylates of Asp6, 55, 62, 71 and 93 and Glu91, the methylthio group of Met13 and the C-terminus carboxylate group (Lys128). Furthermore, relatively high negative peaks developed on specific nitrates from the crystallization solution and water molecules. The only disulphide bridge between Cys3 and Cys26 is almost untouched; similarly copper ligand Cys112 seems to be little affected by radiation damage. In myoglobin

the highest peaks were found in Asp20 and 109 and Glu27, 83 and 105. One methionine (Met131) is also affected, but to a lesser extent than most of the acidic residues. The water coordinated to the haem-bound iron is partially lost. These observations suggest that S–S bonds are more readily protected by scavengers compared with carboxylate groups, corroborating the findings observed in the study by Kauffmann *et al.* (2006).

Average peak heights at carboxylates and sulphurs mostly increase smoothly from difference map $|F_{o2}| - |F_{o1}|$ to $|F_{o5}| - |F_{o1}|$ (Fig. 8).

Peak heights in $\text{e} \text{ \AA}^{-3}$ are shown in Table 4 for the nine azurin and two myoglobin data sets. Results for azurin confirm the protective effect of SAA and suggest HEP and DNQ as possible further candidates to be used as scavengers in macromolecular experiments. Myoglobin peak heights would indicate NSA to be protecting against radiation damage at the concentrations used, but the limited quantity of data available highlights that further testing is necessary.

4. Conclusions

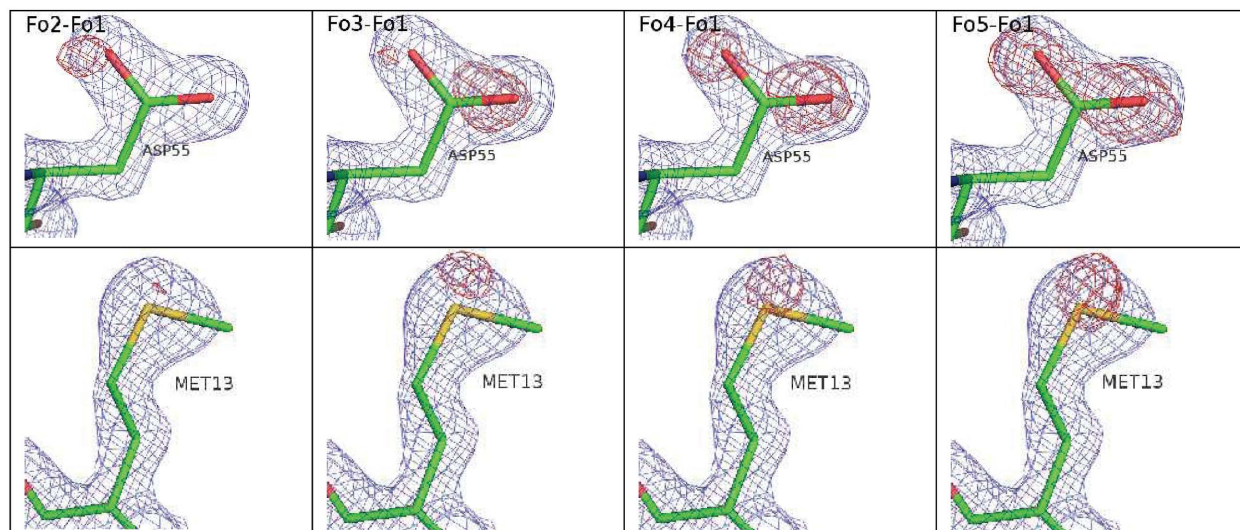
X-ray crystallography data from azurin crystals confirm ascorbate (SAA) as an efficient protecting agent against global and specific radiation damage effects and suggests HEPES (HEP) and 2,3-dichloro-1,4-naphthoquinone (DNQ) as further potential candidates based on peak height changes in electron density difference maps.

The fast X-ray-induced reduction of the copper and iron centres in azurin and myoglobin, respectively, was monitored by on-line microspectrophotometry, as classical X-ray diffraction approaches neither allows for required time resolution nor for discerning often subtle structural differences resulting from metal reduction. The analysis of the spectroscopic data reported here consistently showed that a pronounced reduction of the metal centre (Fe^{3+} or Cu^{2+}) takes place in the first minute of exposure to X-rays at a third-generation synchrotron source, after absorption of a dose as small as 0.4 MGy for azurin and 1.0 MGy for myoglobin crystals. The speed of the photoreduction is independent of the presence of most of the 18 screened scavengers at the concentrations tested and absorbed doses. A small mitigating effect can be seen in the case of the transition metal complex hexacyanoferrate(III) (KF). In the KF-soaked crystal spectra, only rate constant d (slow rate process) contributes to the fit of the amplitude decay curve (contribution of b being negligible). Looking exclusively at d as a metric, scavengers such as sodium salicylate (NSA), HEPES (HEP), thiourea (TU) and ascorbate (SAA) emerge as promising, which is consistent with the results obtained from crystallographic data analysis.

Owing to the fast initial reduction it seems improbable that any concentration of the tested scavengers can efficiently protect the metal centres of metalloproteins. The doses absorbed by a crystal during standard collection of a complete data set are about an order of magnitude higher than the doses used in this study. The small effect seen for the most efficient scavengers would not allow the collection of a full data set

Table 4Average heights of peaks close to carboxylates or sulphurs in $|F_{ox}| - |F_{o1}|$ maps for azurin and myoglobin.The values are the average calculated from all molecules in the asymmetric unit and are given in $e \text{ \AA}^{-3}$.

	Azurin								Myoglobin		
	Native	Native-2	Cysteine	DNQ	Hepes	NA	NI	SAA	TU	Native	NSA
$F_{o2} - F_{o1}$	0.088	0.078	0.080	0.093	0.077	0.121	0.080	0.067	0.109	0.036	0.066
$F_{o3} - F_{o1}$	0.092	0.095	0.091	0.098	0.083	0.098	0.097	0.079	0.113	0.082	0.052
$F_{o4} - F_{o1}$	0.106	0.121	0.102	0.096	0.121	0.175	0.124	0.097	0.131	0.084	0.069
$F_{o5} - F_{o1}$	0.112	0.146	0.179	0.110	0.129	0.179	0.154	0.122	0.149	0.103	0.089

**Figure 8**

Difference electron density peaks growing with increasing applied dose from map $|F_{o2}| - |F_{o1}|$ (left-most figure) to $|F_{o5}| - |F_{o1}|$ (right-most figure). The $2|F_o| - |F_c|$ map (blue) is contoured at 1σ , the $|F_{ox}| - |F_{o1}|$ map (red) at 3σ . The figure was generated from the native-2 data of azurin and shows residues Asp55 and Met13. [Figure created using PyMOL (DeLano, 2000).]

from a single crystal in a fully oxidized state. The findings presented here indicate that interpretation of structural data from redox-sensitive metalloproteins collected on high-brilliance synchrotron sources demands special attention and strongly suggest spectroscopic monitoring of the oxidation state of the metal, use of a composite data collection strategy (Berglund *et al.*, 2002; Yano *et al.*, 2005; Wuergeles *et al.*, 2004) and/or liquid-helium-based cooling which can reduce the reduction rate (Corbett *et al.*, 2007) as the best combined approach currently at hand to determine metal site structures in their native state.

The authors would like to thank Dr Xavier Thibault for help with the photodiode used for the measurement of the photon flux delivered to the samples, and Dr Elspeth Garman for comments on the manuscript. This work has been supported by the European Commission 6th Framework Programme 'Life Sciences, Genomics and Biotechnology for Health' (Integrated Research Project BIOXHIT, Contract No. LSHG-CT-2003-503420). We gratefully acknowledge the ESRF (MX504, MX614, MX637) for providing beam time.

References

- Adam, V., Royant, A., Nivière, V., Molina-Heredia, F. P. & Bourgeois, D. (2004). *Structure*, **12**, 1729–1740.
- Adman, E. T., Stenkamp, R. E., Sieker, L. C. & Jensen, L. H. (1978). *J. Mol. Biol.* **123**, 35–47.
- Beitlich, T., Kühnel, K., Schulze-Briese, C., Shoeman, R. L. & Schlichting, I. (2007). *J. Synchrotron Rad.* **14**, 11–23.
- Berglund, G. I., Carlsson, G. H., Smith, A. T., Szöke, H., Henriksen, A. & Hajdu, J. (2002). *Nature (London)*, **417**, 463–468.
- Blake, C. C. & Phillips, D. C. (1962). *Proceedings of the Symposium on the Biological Effects of Ionizing Radiation at the Molecular Level*, Vienna, Austria, pp. 183–191.
- Bourgeois, D., Vernede, X., Adam, V., Fioravanti, E. & Ursby, T. (2002). *J. Appl. Cryst.* **35**, 319–326.
- Burmeister, W. P. (2000). *Acta Cryst.* **D56**, 328–341.
- Collaborative Computational Project, Number 4 (1994). *Acta Cryst.* **D50**, 760–763.
- Colletier, J.-P., Bourgeois, D., Fournier, D., Silman, I., Sussman, J. L. & Weik, M. (2009). *Proc. Natl Acad. Sci. USA*. In the press.
- Corbett, M. C., Latimer, M. J., Poulos, T. L., Sevioukova, I. F., Hodgson, K. O. & Hedman, B. (2007). *Acta Cryst.* **D63**, 951–960.
- DeLano, W. L. (2000). *PyMOL*, <http://www.pymol.org/>.
- Dennison, C. (2005). *Coord. Chem. Rev.* **249**, 3025–3054.
- Diederichs, K. (2006). *Acta Cryst.* **D62**, 96–101.
- Dubnovitsky, A. P., Ravelli, R. B., Popov, A. N. & Papageorgiou, A. C. (2005). *Protein Sci.* **14**, 1498–1507.

- Emsley, P. & Cowtan, K. (2004). *Acta Cryst.* **D60**, 2126–2132.
- Evans, P. (2006). *Acta Cryst.* **D62**, 72–82.
- Fioravanti, E., Vellieux, F. M. D., Amara, P., Madern, D. & Weik, M. (2007). *J. Synchrotron Rad.* **14**, 84–91.
- Fulford, J., Nikjoo, H., Goodhead, D. T. & O'Neill, P. (2001). *Int. J. Radiat. Biol.* **77**, 1053–1066.
- Garman, E. (1999). *Acta Cryst.* **D55**, 1641–1653.
- Garman, E. F. & Schneider, T. R. (1997). *J. Appl. Cryst.* **30**, 211–237.
- George, G. N., Hedman, B. & Hodgson, K. O. (1998). *Nat. Struct. Biol.* **5**(Suppl.), 645–647.
- Geremia, S., Campagnolo, M., Demitri, N. & Johnson, L. N. (2006). *Structure*, **14**, 393–400.
- Gonzalez, A. & Nave, C. (1994). *Acta Cryst.* **D50**, 874–877.
- Hadfield, A. & Hajdu, J. (1993). *J. Appl. Cryst.* **26**, 839–842.
- Helliwell, J. R. (1988). *J. Cryst. Growth*, **90**, 259–272.
- Henderson, R. (1990). *Proc. R. Soc. London*, **241**, 6–8.
- Hope, H. (1988). *Acta Cryst.* **B44**, 22–26.
- Hough, M. A., Antonyuk, S. V., Strange, R. W., Eady, R. R. & Hasnain, S. S. (2008). *J. Mol. Biol.* **378**, 353–361.
- Jones, G. D., Lea, J. S., Symons, M. C. & Taiwo, F. A. (1987). *Nature (London)*, **330**, 772–773.
- Kabsch, W. (1993). *J. Appl. Cryst.* **26**, 795–800.
- Kauffmann, B., Weiss, M. S., Lamzin, V. S. & Schmidt, A. (2006). *Structure*, **14**, 1099–1105.
- Li, C., Yanagisawa, S., Martins, B. M., Messerschmidt, A., Banfield, M. J. & Dennison, C. (2006). *Proc. Natl Acad. Sci. USA*, **103**, 7258–7263.
- Massover, W. H. (2007). *J. Synchrotron Rad.* **14**, 116–127.
- Maurus, R., Overall, C. M., Bogumil, R., Luo, Y., Mauk, A. G., Smith, M. & Brayer, G. D. (1997). *Biochim. Biophys. Acta*, **1341**, 1–13.
- McGeehan, J. E., Ravelli, R. B. G., Murray, J. W., Owen, R. L., Cipriani, F., McSweeney, S. M., Weik, M. & Garman, E. F. (2009). *J. Synchrotron Rad.* **16**, 163–172.
- Mozumder, A. & Magee, J. L. (1966). *Radiat. Res.* **28**, 203–214.
- Murray, J. & Garman, E. (2002). *J. Synchrotron Rad.* **9**, 347–354.
- Murray, J. W., Garman, E. F. & Ravelli, R. B. G. (2004). *J. Appl. Cryst.* **37**, 513–522.
- Murray, J. W., Rudiño-Piñera, E., Owen, R. L., Grininger, M., Ravelli, R. B. G. & Garman, E. F. (2005). *J. Synchrotron Rad.* **12**, 268–275.
- Murshudov, G. N., Vagin, A. A. & Dodson, E. J. (1997). *Acta Cryst.* **D53**, 240–255.
- Nar, H., Messerschmidt, A., Huber, R., van de Kamp, M. & Canters, G. W. (1991). *J. Mol. Biol.* **221**, 765–772.
- Nave, C. (1995). *Radiat. Phys. Chem.* **45**, 483–490.
- Nave, C. & Garman, E. F. (2005). *J. Synchrotron Rad.* **12**, 257–260.
- O'Neill, P., Stevens, D. L. & Garman, E. (2002). *J. Synchrotron Rad.* **9**, 329–332.
- O'Reilly, J. E. (1973). *Biochim. Biophys. Acta*, **292**, 509–515.
- Orpen, A. G., Brammer, L., Allen, F. H., Kennard, O., Watson, D. G. & Taylor, R. (1989). *J. Chem. Soc. Dalton Trans.* pp. S1–S83.
- Owen, R. L., Rudiño-Piñera, E. & Garman, E. F. (2006). *Proc. Natl Acad. Sci. USA*, **103**, 4912–4917.
- Perrakis, A., Morris, R. & Lamzin, V. S. (1999). *Nat. Struct. Biol.* **6**, 458–463.
- Ravelli, R. B. G. & McSweeney, S. M. (2000). *Structure*, **8**, 315–328.
- Sato, M., Shibata, N., Morimoto, Y., Takayama, Y., Ozawa, K., Akutsu, H., Higuchi, Y. & Yasuoka, N. (2004). *J. Synchrotron Rad.* **11**, 113–116.
- Schlichting, I., Berendzen, J., Chu, K., Stock, A. M., Maves, S. A., Benson, D. E., Sweet, R. M., Ringe, D., Petsko, G. A. & Sligar, S. G. (2000). *Science*, **287**, 1615–1622.
- Sherwood, C., Mauk, A. G. & Brayer, G. D. (1987). *J. Mol. Biol.* **193**, 227.
- Sliz, P., Harrison, S. C. & Rosenbaum, G. (2003). *Structure*, **11**, 13–19.
- Sonntag, C. von & Schuchmann, H. P. (1994). *Methods Enzymol.* **233**, 3–21.
- Southworth-Davies, R. J. & Garman, E. F. (2007). *J. Synchrotron Rad.* **14**, 73–83.
- Southworth-Davies, R. J., Medina, M. A., Carmichael, I. & Garman, E. F. (2007). *Structure*, **15**, 1531–1541.
- Vagin, A. & Teplyakov, A. (1997). *J. Appl. Cryst.* **30**, 1022–1025.
- Varadarajan, R., Zewert, T. E., Gray, H. B. & Boxer, S. G. (1989). *Science*, **243**, 69–72.
- Weik, M., Bergès, J., Raves, M. L., Gros, P., McSweeney, S., Silman, I., Sussman, J. L., Houée-Levin, C. & Ravelli, R. B. G. (2002). *J. Synchrotron Rad.* **9**, 342–346.
- Weik, M., Ravelli, R. B. G., Kryger, G., McSweeney, S., Raves, M. L., Harel, M., Gros, P., Silman, I., Kroon, J. & Sussman, J. L. (2000). *Proc. Natl Acad. Sci. USA*, **97**, 623–628.
- Wuerges, J., Lee, J.-W., Yim, Y.-I., Yim, H.-S., Kang, S.-O. & Djinovic Carugo, K. (2004). *Proc. Natl Acad. Sci. USA*, **101**, 8569–8574.
- Yanagisawa, S. & Dennison, C. (2004). *J. Am. Chem. Soc.* **126**, 15711–15719.
- Yano, J., Kern, J., Irrgang, K.-D., Latimer, M. J., Bergmann, U., Glatzel, P., Pushkar, Y., Biesiadka, J., Loll, B., Sauer, K., Messinger, J., Zouni, A. & Yachandra, V. K. (2005). *Proc. Natl Acad. Sci. USA*, **102**, 12047–12052.
- Yonath, A. *et al.* (1998). *Acta Cryst.* **A54**, 945–955.
- Zaloga, G. & Sarma, R. (1974). *Nature (London)*, **251**, 551–552.